# Application and clinical translational value of a predictive model based on $N^7$-methylguanosine-related long non-coding RNAs in cervical squamous cell carcinoma

JUN ZHANG[1-3], YINGNA BAO[3], ZHILONG YU[3] and YU LIN[3]

[1]State Key Laboratory of Reproductive Regulation and Breeding of Grassland Livestock, Inner Mongolia University, Hohhot, Inner Mongolia Autonomous Region 010050, P.R. China; [2]Department of Biochemistry and Molecular Biology, School of Life Sciences, Inner Mongolia University, Hohhot, Inner Mongolia Autonomous Region 010050, P.R. China; [3]Department of Radiotherapy, Affiliated Hospital of Inner Mongolia Medical University, Hohhot, Inner Mongolia Autonomous Region 010050, P.R. China

Received October 20, 2024; Accepted April 4, 2025

DOI: 10.3892/ol.2025.15087

**Abstract.** Cervical squamous cell carcinoma (CSCC) is one of the most common gynecological malignancies affecting women globally. The present study aimed to develop a predictive model based on $N^7$-methylguanosine-related long non-coding RNAs (lncRNAs) to evaluate risk stratification, analyze immune infiltration and guide the selection of sensitive drugs in CSCC. Pearson's correlation, univariate Cox and Least Absolute Shrinkage and Selection Operator regression analyses of transcriptome data from The Cancer Genome Atlas and the Genotype-Tissue Expression database were conducted to construct a prognostic risk prediction model for CSCC. The stability of the model was tested before evaluating its prognostic value in CSCC. Further analysis of enrichment, immune infiltration and drug resistance provided directions for clinical translation. The lncRNAs used to construct the model were validated using reverse transcription-quantitative PCR. The developed predictive model was stable and may hold notable clinical translational value for immunotherapy and drug selection in CSCC in the future.

## Introduction

Cervical squamous cell carcinoma (CSCC) is one of the most common gynecological cancer types affecting women worldwide. The International Agency for Research on Cancer (IARC) reported that there were 60,412 new cases of cervical cancer in 2020, which resulted in 341,831 deaths (1). The high-risk human papillomavirus continues to be the primary pathogen responsible for CSCC (2). Epigenetic modifications, including DNA methylation, histone modification, non-coding RNA regulation and chromatin remodeling, are closely associated with the development of CSCC (3). However, these mechanisms do not fully elucidate the pathogenesis of CSCC, necessitating further exploration of treatment strategies based on epigenetic modifications.

The most prevalent and reversible RNA alteration found in mammals is the $N^6$-methyladenosine ($m^6A$) modification (4). Other types of RNA modification, such as the $N^7$-methylguanosine ($m^7G$) modification, which is mainly defined by the creation of a 'cap' structure at the 5'-untranslated region of mRNA, transfer RNA (tRNA), ribosomal RNA (rRNA) and microRNA (miRNA/miR), have also received attention recently (5,6). Methyltransferase 1 (METTL1) and its cofactor, WD repeat domain 4 (WDR4), together form the METTL1/WDR4 complex, which is the most extensively researched regulatory component of $m^7G$ modification. The METTL1/WDR4 complex is essential for the biological roles of $m^7G$ modification across tRNA, rRNA, miRNA and mRNA (7). For example, METTL1 modifies the $m^7G$ modification of rRNA in bladder cancer, regulating the ribosome during tRNA-mRNA codon recognition (8). Furthermore, METTL1 knockdown markedly increases the sensitivity of HeLa cells to 5-fluorouracil, suggesting that $m^7G$ alteration is a viable target to overcome tumor cell resistance (9). By controlling the $m^7G$ alteration of tRNA, the METTL1/WDR4 complex increases the production of EGFR protein in hepatocellular carcinoma, reducing the susceptibility of liver cancer cells to Lenvatinib (10). Aberrant $m^7G$ alteration is frequently linked to a variety of tumor outcomes, including the promotion of bladder, liver and head and neck cancer progression and the possible inhibition of teratoma progression (11,12). However, it is currently unclear how the $m^7G$ mutation affects the development of cervical cancer.

Numerous non-coding RNA functions have been identified as high-throughput sequencing technologies have advanced (13). Transcripts >200 nucleotides, known as long non-coding RNAs (lncRNAs) (14), are essential for vital biological processes at the transcriptional, translational

*Correspondence to:* Dr Yu Lin, Department of Radiotherapy, Affiliated Hospital of Inner Mongolia Medical University, 1 North Tongdao Road, Huimin, Hohhot, Inner Mongolia Autonomous Region 010050, P.R. China
E-mail: honglanqian@126.com

*Key words:* cervical squamous cell carcinoma, $N^7$-methylguanosine, long non-coding RNA, predictive model, immune infiltration

and post-translational stages (15). In the field of oncology, lncRNAs modulate the expression of target genes in tumors, thereby altering the biological behaviors of cancer cells (16). Previous research has demonstrated the key roles that lncRNAs serve in cervical cancer growth, metastasis, drug resistance, immuno-environmental changes and metabolic reprogramming (17). Compared with proteins, lncRNAs are highly specialized. Novel techniques for targeted therapy can be derived from clustering tumor subtypes based on the differential expression patterns of lncRNAs (18-20). According to an analysis of The Cancer Genome Atlas (TCGA), the expression levels of lncRNAs are frequently dysregulated in cancer and has the highest cancer type-specificity, followed by pseudogenes and then protein-coding genes, which were least subtype specific and ~18.27% of lncRNAs showed subtype specificity, while only 10.55% of protein-coding genes were subtype-specific (21-24). Therefore, from this perspective, dysregulated lncRNAs hold greater specificity for tumor diagnosis and classification compared with protein-coding genes, which adds further importance to the identification of specific lncRNAs as tumor biomarkers.

To the best of our knowledge, research on lncRNAs linked to the $m^7G$ modification in CSCC has not yet been conducted. Therefore, the aim of the present study was to identify $m^7G$-related lncRNAs and build prognostic, immune infiltration and drug-sensitivity models around them, which may be valuable for CSCC genotyping, diagnosis and prognostic evaluation in the future.

## Materials and methods

*Datasets*. Transcriptome data and clinical features of patients with CSCC and normal individuals were retrieved from TCGA (https://portal.gdc.cancer.gov/) and Genotype-Tissue Expression (GTEx; https://www.genome.gov/Funded-Programs-Projects/Genotype-Tissue-Expression-Project; GTEx_Analysis_2017-06-05_v8_RNASeQCv1.1.9_gene_reads.gct.gz) databases and a dataset of 260 samples, which included 248 cancerous tissues and 12 normal tissues or adjacent non-cancerous tissues. Furthermore, 35 $m^7G$-related genes were gathered from the Gene Set Enrichment Analysis (GSEA; https://www.gsea-msigdb.org/gsea/index.jsp) website and relevant published literature (25).

The present research was not subject to ethical committee review as all data was obtained from publicly accessible databases.

*Identification of $m^7G$-related lncRNAs*. Gene annotation probes for the expression matrix were downloaded from GENCODE (https://www.gencodegenes.org/). Differential analysis was performed using the 'limma' package (RStudio; Posit Software, PBC) to obtain differentially expressed $m^7G$-related genes and lncRNAs, with the criteria of $|\log_2[\text{fold change (FC)}]|>2$ and false discovery rate (FDR) <0.05. The differentially expressed genes (DEGs) underwent Pearson's correlation coefficient analysis ($r^2$) and lncRNAs meeting the criteria of |coefficients|>0.4 and P<0.05 were defined as $m^7G$-related lncRNAs.

*Development of a prediction model based on $m^7G$-related lncRNAs*. Integration of $m^7G$-related lncRNAs along with survival durations and statuses, among other clinical data was conducted. Univariate Cox analysis was conducted using the 'Survival' package (RStudio; Posit Software, PBC). Least Absolute Shrinkage and Selection Operator (LASSO) regression analysis was performed using the 'glmnet' package (RStudio; Posit Software, PBC), culminating in a predictive model after 10-fold cross-validation. The formula was as follows:

$$\text{Risk score} = \sum_{i=0}^{n} \text{Coefi} \times \text{Expi}$$

The survival correlation regression coefficient was denoted by Coefi. The expression value of each $m^7G$-related lncRNA was denoted by Expi.

*Application of the prediction model in CSCC prognosis*. The 'Survival' package was employed to generate the overall survival (OS) curve for CSCC. The 'pROC' package facilitated the appraisal of clinicopathological characteristics and prognostic implications through the computation of the area under the curve (AUC) and utilizing the 'rms' package, a nomogram was constructed and calibration curves were plotted to gauge the predictive efficacy of the model across the aggregate sample.

*GSEA and Kyoto Encyclopedia of Genes and Genomes (KEGG) enrichment analysis*. The 'msigdbr' package (RStudio; Posit Software, PBC) was utilized for GSEA, with minimum and maximum values of gene expression profiles set at 10 and 500 respectively, and 1,000 resampling iterations conducted. An FDR <0.25 and P<0.05 were considered to indicate statistical significance. Pathway enrichment analysis was performed using the 'clusterProfiler' package in conjunction with KEGG analysis (http://www.genome.jp/kegg/). Visualization was achieved through the use of the 'ggplot2' package (RStudio; Posit Software, PBC).

*Immune feature analysis*. The 'CIBERSORT' package (RStudio; Posit Software, PBC) was used to integrate transcriptomic data with the expression of immune cell marker genes, which yielded an infiltrative distribution score of immune cells within tumor tissues. Employing 1,000 permutations of the default matrix to ascertain P-values for each specimen, the infiltration of immune cells in the cohort was evaluated, with P<0.05 considered statistically significant. The 'ggplot2' and 'barplot' packages (Posit Software, PBC) were utilized to visually represent the data.

*Drug sensitivity evaluation*. The 'pRRophetic' package (RStudio; Posit Software, PBC) was used to evaluate the treatment efficacy for patients with CSCC in high- and low-risk subgroups based on the $IC_{50}$. Subsequently, data visualization was performed using R packages such as 'ggplot2' and 'barplot' (Posit Software, PBC).

*RNA isolation and reverse transcription-quantitative PCR (RT-qPCR) (26)*. Human cervical cancer cell lines (SiHa and HeLa cells) and the human cervical epithelial cell line H8 (cat. no. BFN607200572) were obtained from the Shanghai Cell Bank (http://www.bluefcell.com). Cels were cultured in

Table I. Primer sequences for reverse transcription-quantitative PCR.

| Gene | Sequence (5'-3') |
|---|---|
| Family with sequence similarity 13 member A AS.1 | F: CAAATATGGGTAAGGAGG |
| | R: GTTTAGAACTATGAGGGACT |
| Family with sequence similarity 27 member E3 AS1 | F: CACTTGAGAAACAGACCGTATTGT |
| | R: CTAGGATCAAGATGAACACACTGC |
| Fibroblast growth factor 13 AS1 | F: AAGAATGGCGGGGGCATTTA |
| | R: CCCCTCCCCCATACTCTTCA |
| Long intergenic non-protein coding RNA 1089 | F: TTTTGCCTACCCAACCCTGG |
| | R: CCTGCCGTTGACAGAAGGAA |
| RBAK downstream neighbor | F: TGGCTGTATTGATGGGGCTG |
| | R: ACAGGGAAAGCCCCATGTTC |
| Solute carrier family 8 member A1 AS1 | F: GCATATGTTGATGAGCAGGCA |
| | R: AGACTCAGTGACAGGGCTCA |
| β-actin | F: AGCGAGCATCCCCCAAAGTT |
| | R: GGGCACGAAGGCTCATCATT |

F, forward; R, reverse; AS1, antisense RNA 1.

1640 medium (containing 10% FBS and 1% streptomycin), at 37˚C and 5% $CO_2$, in a humidified incubator with saturated humidity. RT-qPCR was conducted to validate the expression levels of the identified $m^7G$-related lncRNAs. TRIzol® (cat. no. 262307; Thermo Fisher Scientific, Inc.) was used to extract total cellular RNA. Subsequently, total RNA was reverse-transcribed using the PrimeScript™ RT reagent kit (cat. no. RR037A; Takara Bio, Inc.). The thermocycling conditions used were as follows: 37˚C for 15 min, 85˚C for 5 sec and 4˚C indefinitely. Amplification was performed using TB Green™ Premix Ex Taq™ II (cat. no. RR820A; Takara Bio, Inc.) on an ABI 7,500 detection system (Thermo Fisher Scientific, Inc.). The thermocycling conditions used were as follows: 95˚C for 30 sec; 40 cycles of 95˚C for 5 sec, 60˚C for 34 sec; and 95˚C for 15 sec, 60˚C for 1 min and a final extension of 95˚C for 15 sec. β-actin was used as the internal reference and the relative expression levels of the target genes were calculated using the $2^{-\Delta\Delta Cq}$ method (26). Primer sequences are listed in Table I.

*Statistical analysis*. Data analysis was primarily conducted using R (version 4.3.2; Posit Software, PBC). LncRNAs closely associated with $m^7G$-related genes were defined as $m^7G$-related lncRNAs based on Pearson's correlation coefficient analysis ($r^2$), with the criteria of |Pearson R|>0.6 and P<0.05.The present study employed univariate Cox regression, LASSO regression, log-rank test, receiver operating characteristic and principal component analysis (PCA) analysis, with unpaired t-tests used for comparisons between high- and low-risk groups. All experiments were repeated three times. One-way ANOVA was used for the analysis of lncRNAs in multiple group comparisons at different tumor staging, while Dunnett's post hoc test after one-way ANOVA was used for the analysis of lncRNAs between different cell lines. Data are presented as the mean ± SD. P<0.05 was considered to indicate a statistically significant difference.

## Results

*Identification of 16 $m^7G$-related lncRNAs in CSCC*. In the present study, data from 260 samples were collected from the TCGA and GTEx databases, comprising 248 tumor samples and 12 control samples. PCA demonstrated a distinct separation between the groups (Fig. 1A). Integrating data from GSEA database and prior literature (27), 35 $m^7G$-related genes were included (Table SI). Consequently, 16 $m^7G$-related lncRNAs for CSCC were identified (Fig. 1B), with 8 upregulated DEGs (NUDT1, NCBP3, WDR4, NCBP2, NCBP1, NUDT5, METTL1 and NUDT7) and 8 downregulated DEGs (EIF4A1, NUDT3, NUDT4, LSM1, NUDT10, SNUPN, EIF4E and NUDT16; P<0.05). lncRNA information was extracted from TCGA and GTEx databases and 1,382 differentially expressed lncRNAs (DELs) were obtained based on the criteria of |log2(FC)|>2 and P<0.05 (Table SII). Heatmaps were generated to display the top 20 upregulated and downregulated DELs (Fig. 1C). Correlation analysis of the DEGs and DELs was performed to identify $m^7G$-related lncRNAs. Pearson's correlation analysis was used to identify 203 DELs that were significantly correlated (P<0.05) with $m^7G$-related lncRNAs (Table SIII; Fig. 1D and E).

*Establishment of a prediction model based on $m^7G$-related lncRNAs*. A univariate Cox analysis of 204 $m^7G$-related lncRNAs and survival data was conducted, where 22 lncRNAs with independent predictive efficacy were identified and shown in a forest plot (Fig. 2A). Following LASSO regression analysis, 6 significant $m^7G$-related lncRNAs were identified: Family with sequence similarity 13 member A antisense RNA 1 (FAM13A.AS1), family with sequence similarity 27 member E3 (FAM27E3), fibroblast growth factor 13 antisense RNA 1 (FGF13.AS1), long intergenic non-protein coding RNA 1089 (LINC01089), RBAK downstream neighbor (RBAKDN) and solute carrier family 8 member A1 antisense RNA 1

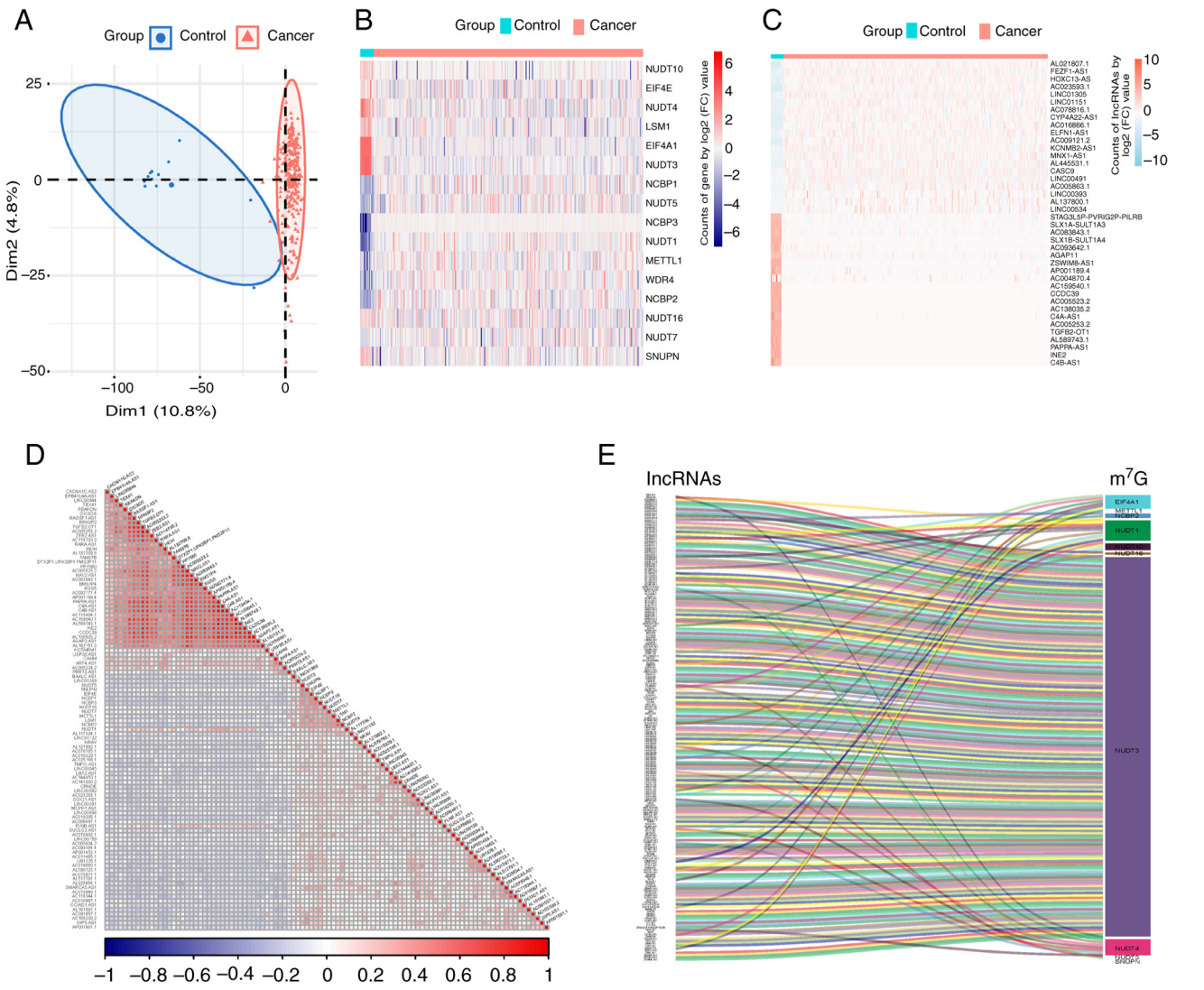


Figure 1. Identification of m$^7$G-related lncRNAs in cervical squamous cell carcinoma. (A) Principal component analysis clustering all selected samples, with tumor tissue samples in red and samples from the healthy control group in blue. (B) Heatmap of 16 m$^7$G-associated DEGs, with higher expression in red and lower expression in blue. (C) Heatmap of DELs showcasing the top 20 DELs, with higher expression in red and lower expression in blue. (D) Correlation heatmap of DEGs and DELs, with positive correlations in red and negative correlations in blue. (E) Sankey diagram showing the 204 DELs significantly correlated with the m$^7$G genes. DEG, differentially expressed gene; lncRNA, long non-coding RNA; DEL, differentially expressed lncRNAs; m$^7$G, N$^7$-methylguanosine; Dim1, dimension 1 formed after data dimensionality reduction; Dim2, dimension 2 formed after data dimensionality reduction.

(SLC8A1.AS1; Fig. 2B). The predictive model was constructed with the following formula: Risk score=(3.24 x FAM13A.AS1) + (-3.07 x FAM27E3) + (2.94 x FGF13.AS1) + (-3.49 x LINC01089) + (3.23 x RBAKDN) + (2.86 x SLC8A1.AS1). Sample risk scores were calculated using this formula and samples were grouped into high- and low-risk groups according to the median score of 1.181 (Fig. 2C). The OS of patients was analyzed using Kaplan-Meier analysis and survival curves were plotted. The outcome demonstrated that the prognosis of the low-risk group significantly improved compared with that of the high-risk group (P<0.0001; Fig. 2D).

*Comparison of clinical characteristics between groups.* One-way ANOVA indicated no significant differences in age, TNM or International Federation of Gynecology and Obstetrics (FIGO) staging between the groups (Fig. 3A). To further examine potential associations between clinical factors and m$^7$G-related lncRNAs, one-way ANOVA was used. Significant differences were observed in the expression levels of LINC01089, FAM13A.AS1, FAM27E3, and FAM13.AS1 across different T stages (P<0.05), with the expression levels of FAM13A.AS1 also showing significant differences across different N stages (P<0.05) and the expression levels of LINC01089, FAM13.AS1 and RBAKDN showing significant differences across different M stages (P<0.05). Additionally, FAM13A.AS1 and FAM13.AS1 expression exhibited significant differences across different FIGO stages (P<0.05; Fig. 3B-E). Based on these findings, it was evident that FAM13A.AS1 and FAM13.AS1 exhibited notable differences across various clinical parameters, underscoring their pivotal roles as principal predictive biomarkers.

*Prediction model serves as an independent risk factor for the prognosis of CSCC.* To validate whether the risk prediction model serves as an independent prognostic factor for cervical cancer, univariate and multivariate Cox regression analyses

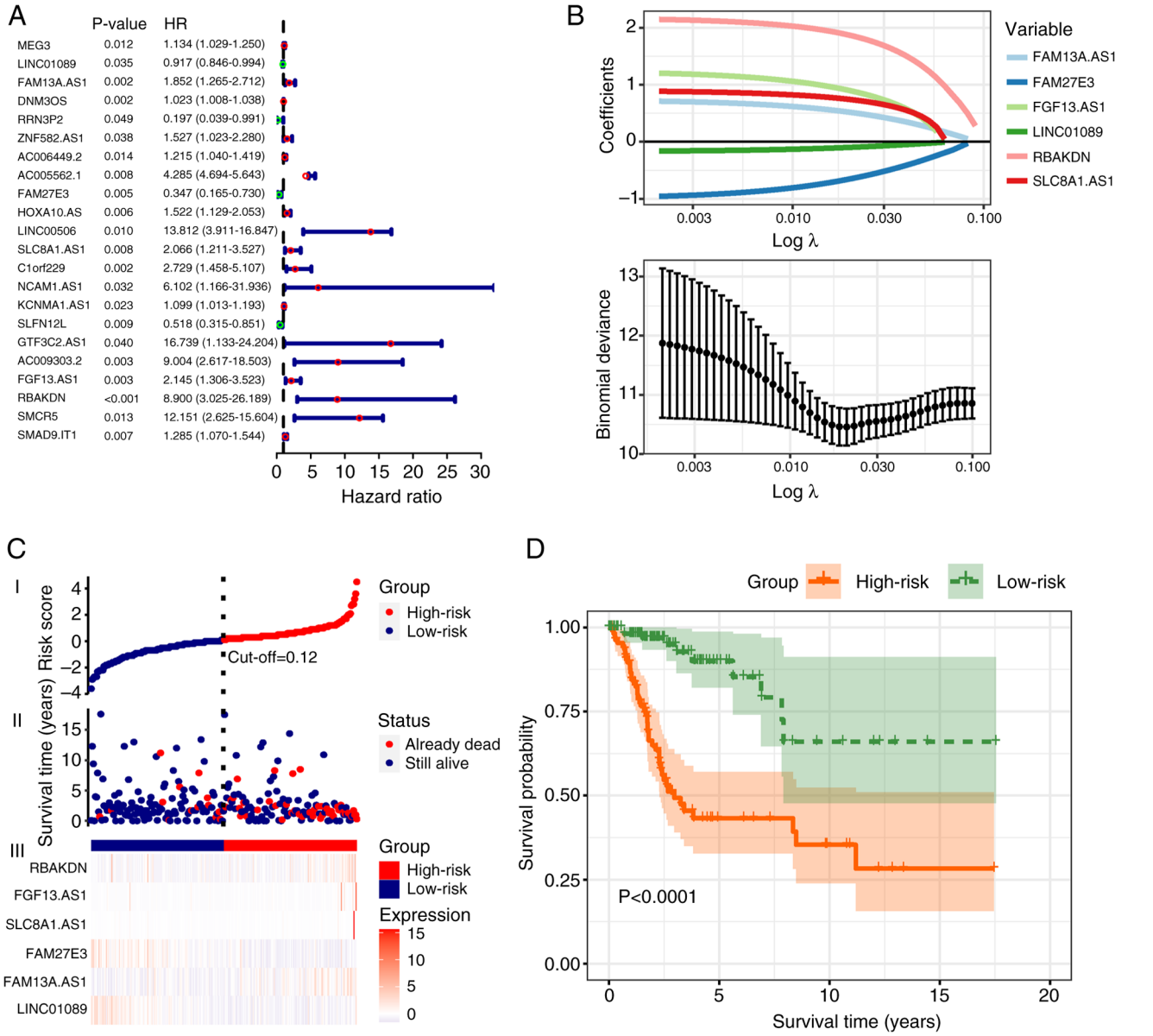


Figure 2. Establishment of a predictive model based on m$^7$G-related lncRNAs. (A) Forest plot illustrating the univariate Cox analysis used to identify 22 m$^7$G-related lncRNAs with independent prognostic prediction capabilities. The results are expressed using hazard ratios (95% CI). (B) Least Absolute Shrinkage and Selection Operator regression plot. Binomial deviances are expressed as mean ± SD. (C) Scatter plot and risk heatmap. The optimal cut-off value was determined to be 0.12, which distinguished the high-risk group (red) from the low-risk group (blue). (D) Kaplan-Meier survival curves. The green curve represents the low-risk group, whereas the orange curve represents the high-risk group. The survival rate of the high-risk group was found to be lower compared to that of the low-risk group. m$^7$G, N$^7$-methylguanosine; lncRNA, long non-coding RNA; AS1, antisense RNA 1; FAM13A.AS1, family with sequence similarity 13 member A AS.1; FAM27E3, family with sequence similarity 27 member E3 AS1; FGF13.AS1, fibroblast growth factor 13 AS1; LINC01089, long intergenic non-protein coding RNA 1089; RBAKDN, RBAK downstream neighbor; SLC8A1.AS1 solute carrier family 8 member A1 AS1.

were conducted using age, TNM stage, FIGO stage and model scores as covariates and the prognostic outcomes as the independent variable. The results demonstrated that the hazard ratio (HR) of the model score was 1.10 (P<0.001; Fig. 4A and B), suggesting that the model score could be considered an independent prognostic risk factor for CSCC. Furthermore, a nomogram was constructed to evaluate the predictive efficiency of each factor (Fig. 4C). The calibration curves plotted demonstrated the normogram-predicted probability, indicating good model calibration and reliability of the predictive performance (Fig. 4D). Compared with age or TNM staging, the model score achieves a higher AUC value (AUC=0.91) (Fig. 4E). Based on the prognostic times assessed using the model, the AUC for 1-, 3- and 5-year survival was 0.8, 0.91 and 0.85, respectively (Fig. 4F), which indicated a commendable predictive performance. These results suggested that the risk prediction model, based on m$^7$G-related lncRNAs, exhibited high sensitivity and specificity in forecasting the prognosis of CSCC.

*GSEA and KEGG enrichment analysis*. To elucidate the enrichment processes of DEGs, GSEA was conducted. The analysis indicated disparities in immunological processes such as the defense response to bacteria (enrichment score=1.943; P=0.005), innate immune response (enrichment score=1.668; P=0.037) and humoral immune response (enrichment score=1.646; P=0.045) between groups (Fig. 5A-D). Further

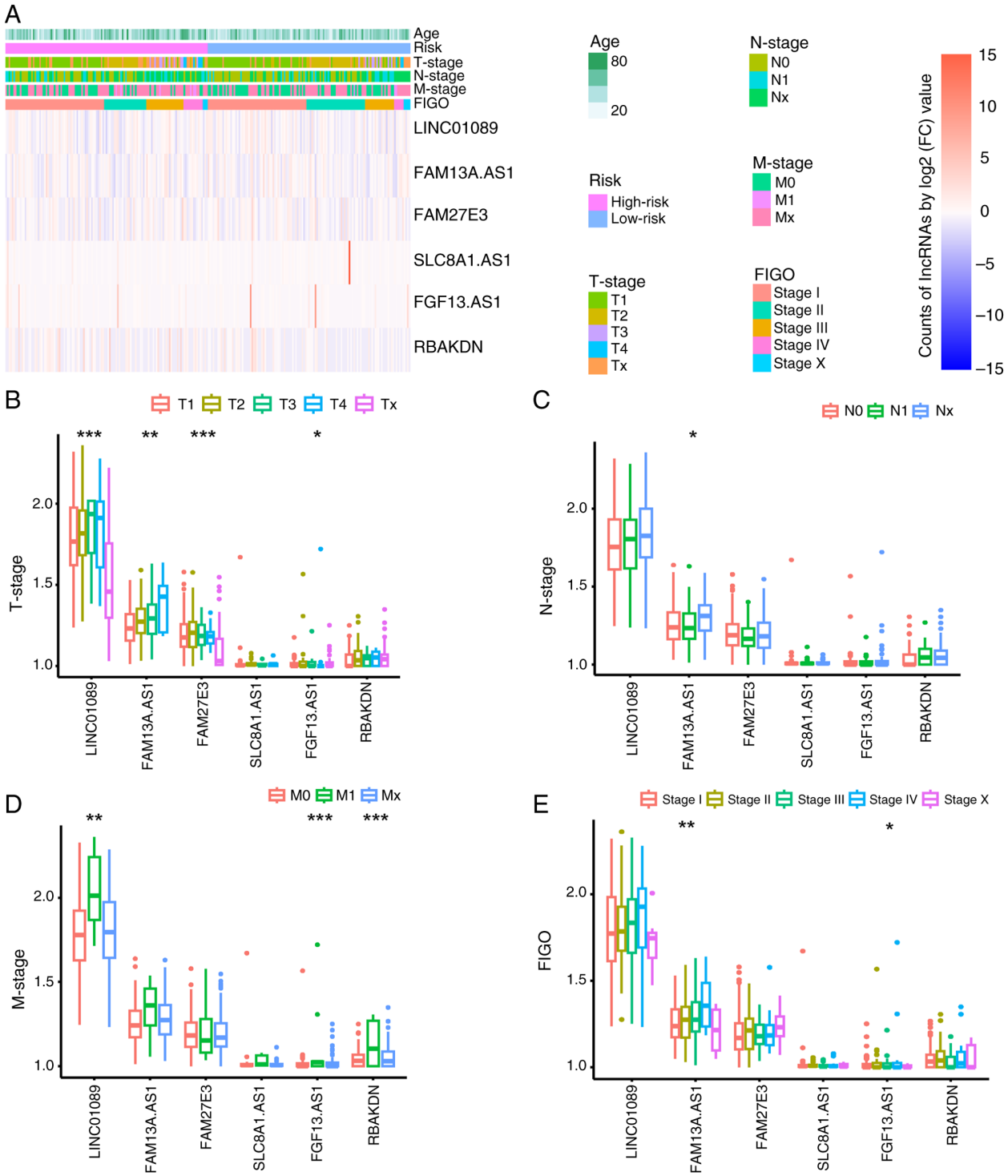


Figure 3. Comparison of clinical characteristics among different groups. (A) Heatmap of age, TNM stage and FIGO stage. (B) Box plot of T-stage stratification. (C) Box plot of N-stage stratification. (D) Box plot of M-stage stratification. (E) Box plot of FIGO stage stratification. $^{*}$P<0.05, $^{**}$P<0.01 and $^{***}$P<0.001. The relative expression levels of lncRNAs are expressed as mean ± SD. FIGO, International Federation of Gynecology and Obstetrics; AS1, antisense RNA 1; FAM13A.AS1, family with sequence similarity 13 member A AS.1; FAM27E3, family with sequence similarity 27 member E3 AS1; FGF13.AS1, fibroblast growth factor 13 AS1; LINC01089, long intergenic non-protein coding RNA 1089; RBAKDN, RBAK downstream neighbor; SLC8A1.AS1 solute carrier family 8 member A1 AS1.

exploration through KEGG analysis highlighted pathways of interest, including transcriptional misregulation in cancer, Ras, Ras-related protein 1 (Rap1) and calcium (Fig. 5E and F).

*Immune infiltration landscape*. The results of GSEA suggested that the progression of CSCC was linked to anomalies in immune responses, particularly innate and humoral immune reactions. Utilizing the 'CIBERSORT' algorithm, the tumor immune microenvironment was compared between high- and low-risk groups. Given the absence of CD4 naïve T cells in any group, the distribution differences of the remaining 21 types of immune cells were examined. Heatmaps and percentage plots

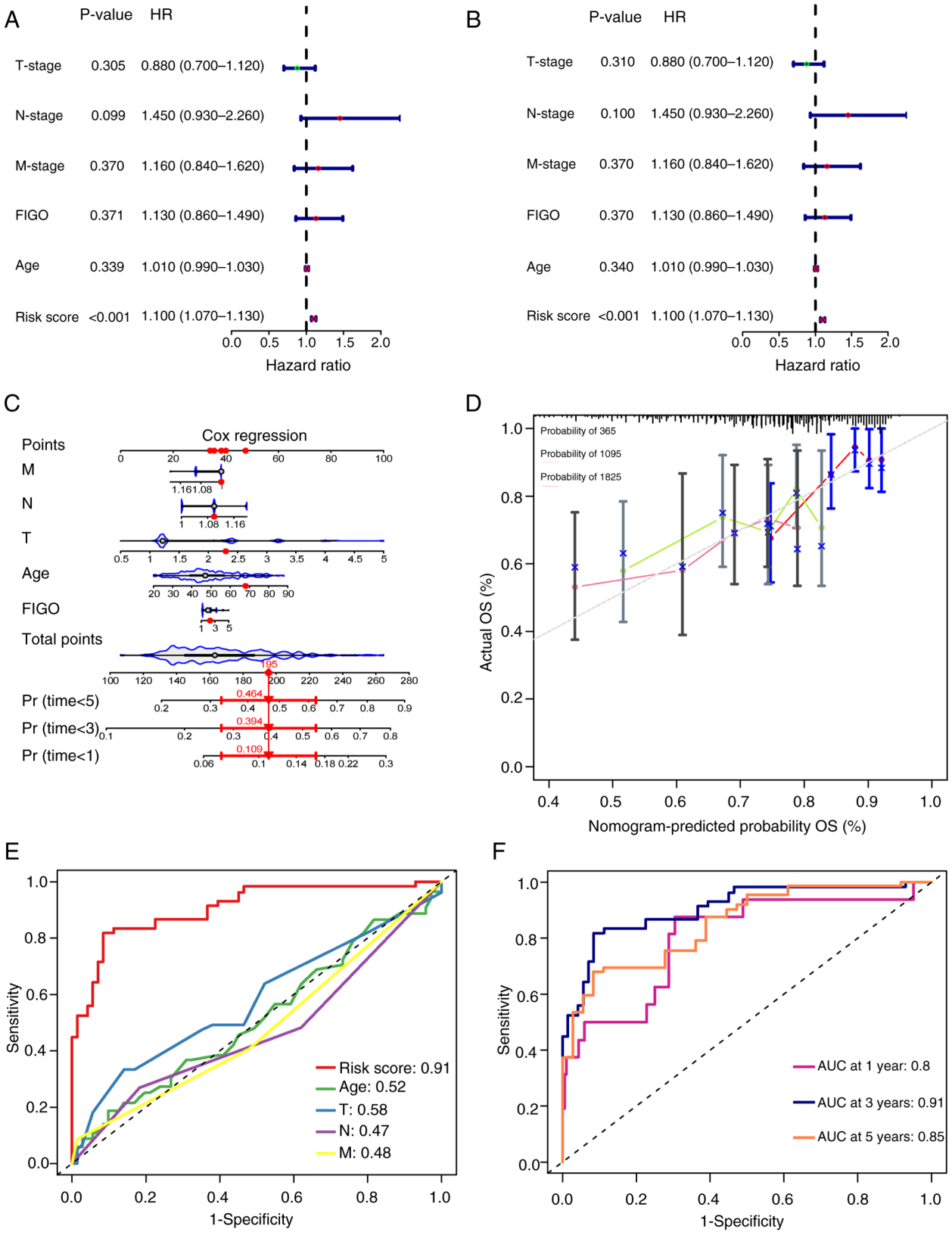


Figure 4. Evaluation of the predictive model and construction of a nomogram. (A) Univariate Cox analysis. The results are expressed using HR (95% CI). (B) Multivariate Cox analysis. HR, 1.10; 95% CI, 1.07-1.13; (C) Nomogram constructed based on clinical factors. (D) Calibration curve for the nomogram. Actual OS (%) is expressed as mean ± SD. (E) The area under the curve of the predictive model was 0.91. (F) Receiver operating characteristic curves corresponding to different survival durations. FIGO, International Federation of Gynecology and Obstetrics; OS, overall survival; HR, hazard ratio; Pr, predicted probability.

demonstrated distinct distributions of immune cells between the groups (Fig. 6A and B). Specifically, mast activated cells exhibited a significantly increased infiltration in the high-risk group (P<0.05), whereas mast resting cells, T regulatory cells,

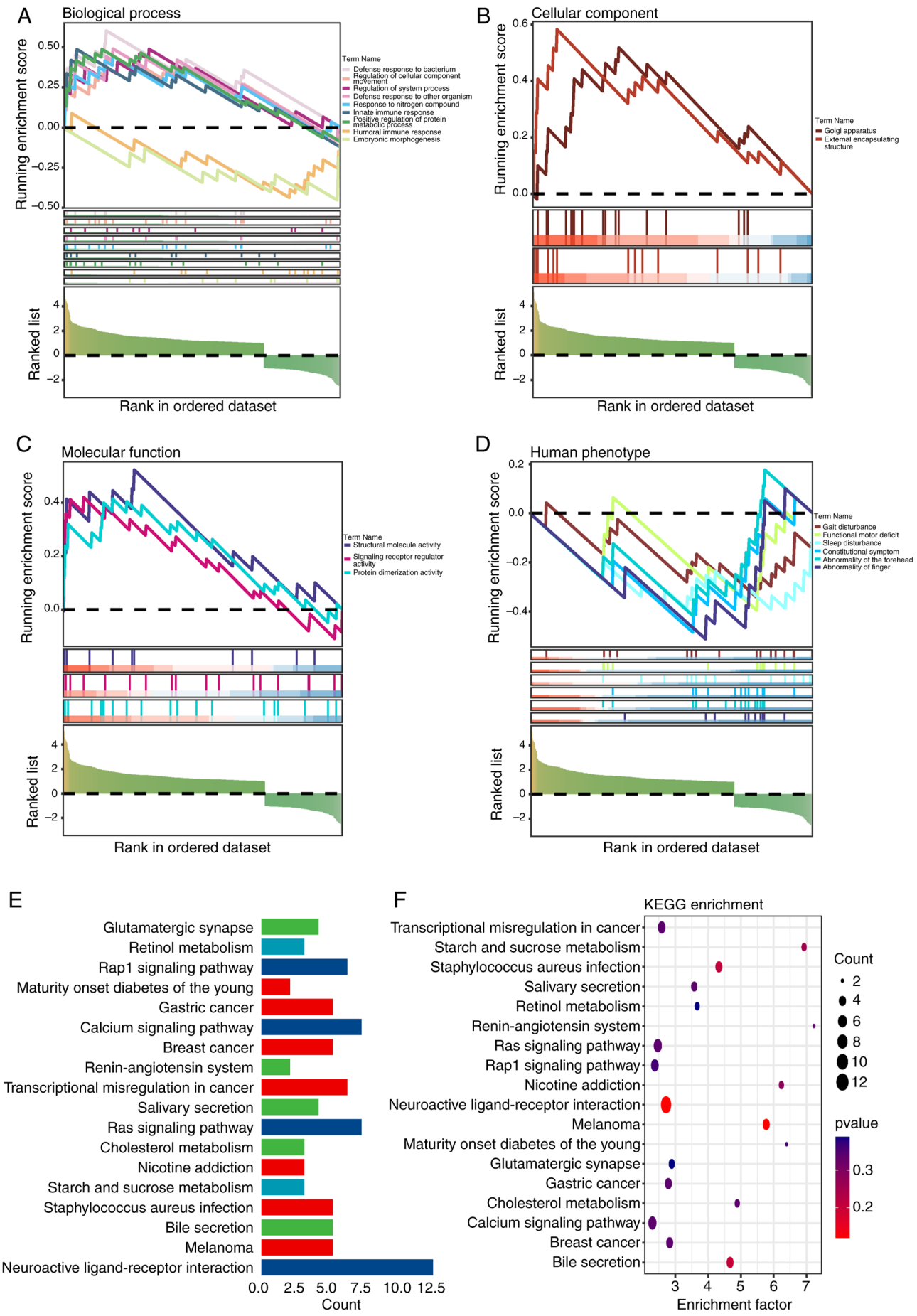


Figure 5. Gene Set Enrichment Analysis and KEGG enrichment analysis. (A) Biological processes. (B) Cellular components. (C) Molecular functions. (D) Human phenotype ontology. (E) KEGG pathway illustration. (F) KEGG bubble chart. KEGG, Kyoto Encyclopedia of Genes and Genomes.

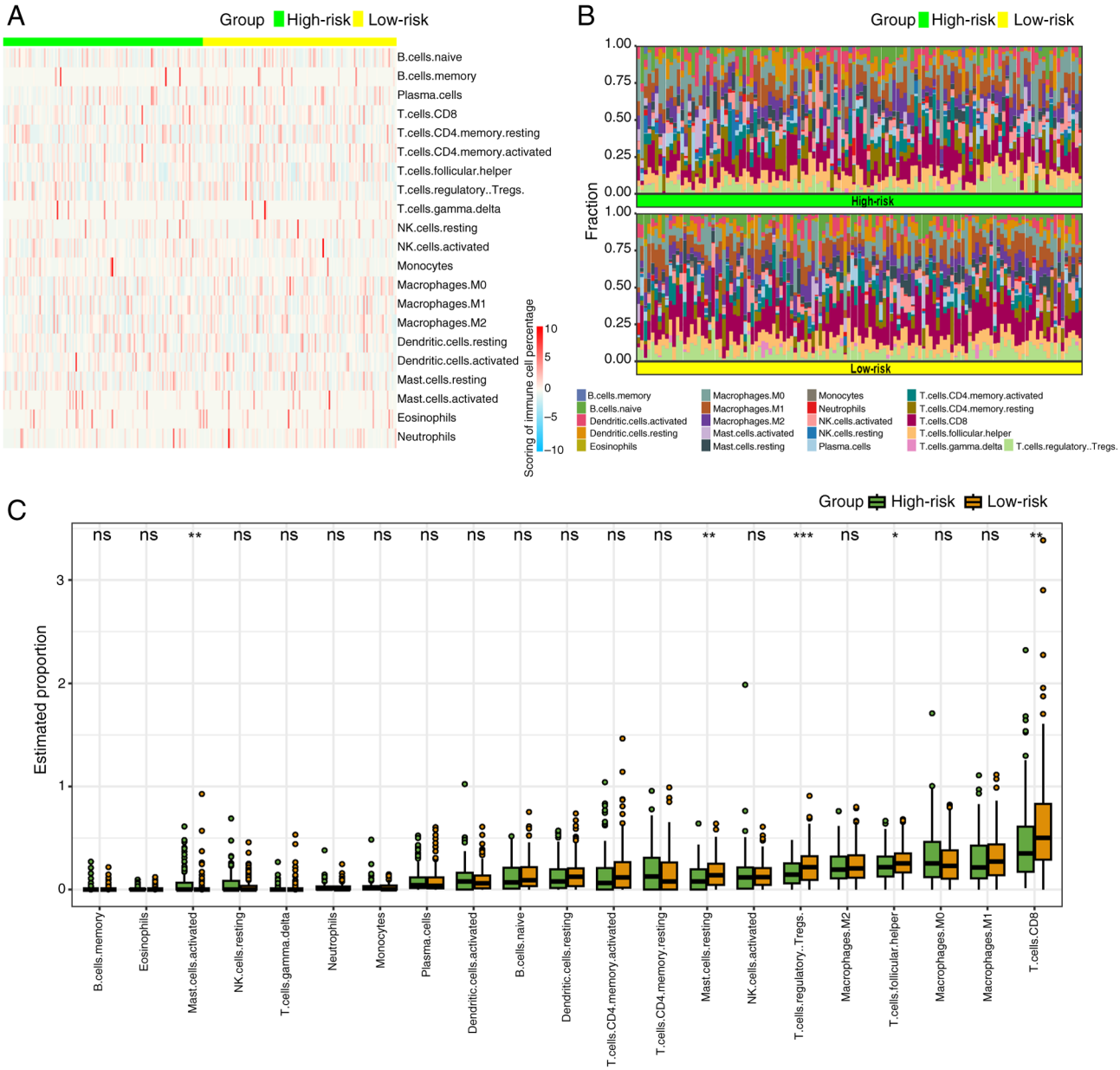


Figure 6. Immune cell infiltration landscape of two groups. (A) Heatmap illustrating the proportions of 21 immune cell types among subgroups. (B) Bar chart depicting the infiltration levels of 21 immune cell types among subgroups. (C) Comparative analysis of the proportion of 21 immune cell types among subgroups, with the high-risk group shown in green and the low-risk group shown in orange. The estimated proportions of various immune cells are expressed as mean ± SD. $^{*}$P<0.05; $^{**}$P<0.01; $^{***}$P<0.001. ns, not significant.

T follicular cells and CD8$^{+}$ T cells showed significantly higher infiltration in the low-risk group (P<0.01, P<0.001, P<0.05 and P<0.01, respectively; Fig. 6C).

*Clinical translational value of prediction models*. To further appraise the clinical applicability and the potential for future clinical translation of the predictive model, the differences in drug sensitivity between groups were analyzed. GSEA and KEGG pathway enrichment analysis results suggested a connection between cervical cancer and abnormalities in transcriptional dysregulation, Ras signaling and other cell cycle proteins. The analysis of drug sensitivity differences demonstrated varying tendencies in the response to drug treatments among different CSCC groups. The high-risk group exhibited a significantly improved responsiveness to the cyclopamine (P<0.05; Fig. 7A), while the low-risk group exhibited higher sensitivity to the Wnt signaling pathway inhibitor FH535, the cell cycle inhibitor vinorelbine, the protein phosphatase 1 (PP1) inhibitor Salubri01, the serine/threonine protein kinase inhibitor CP-466722 and the tyrosine kinase receptor inhibitor crizotinib (Fig. 7B-F).

*Validation of model-constructing lncRNAs through RT-qPCR*. Through analysis of the risk prediction model in terms of clinical data, immune infiltration and drug sensitivity, its substantial applicability in the context of CSCC was discerned. To ascertain the precision and reliability of the lncRNAs implicated in constructing the model, the aforementioned 6 lncRNAs were evaluated using RT-qPCR analysis in H8, SiHa and HeLa cervical cancer cell lines. The expression levels

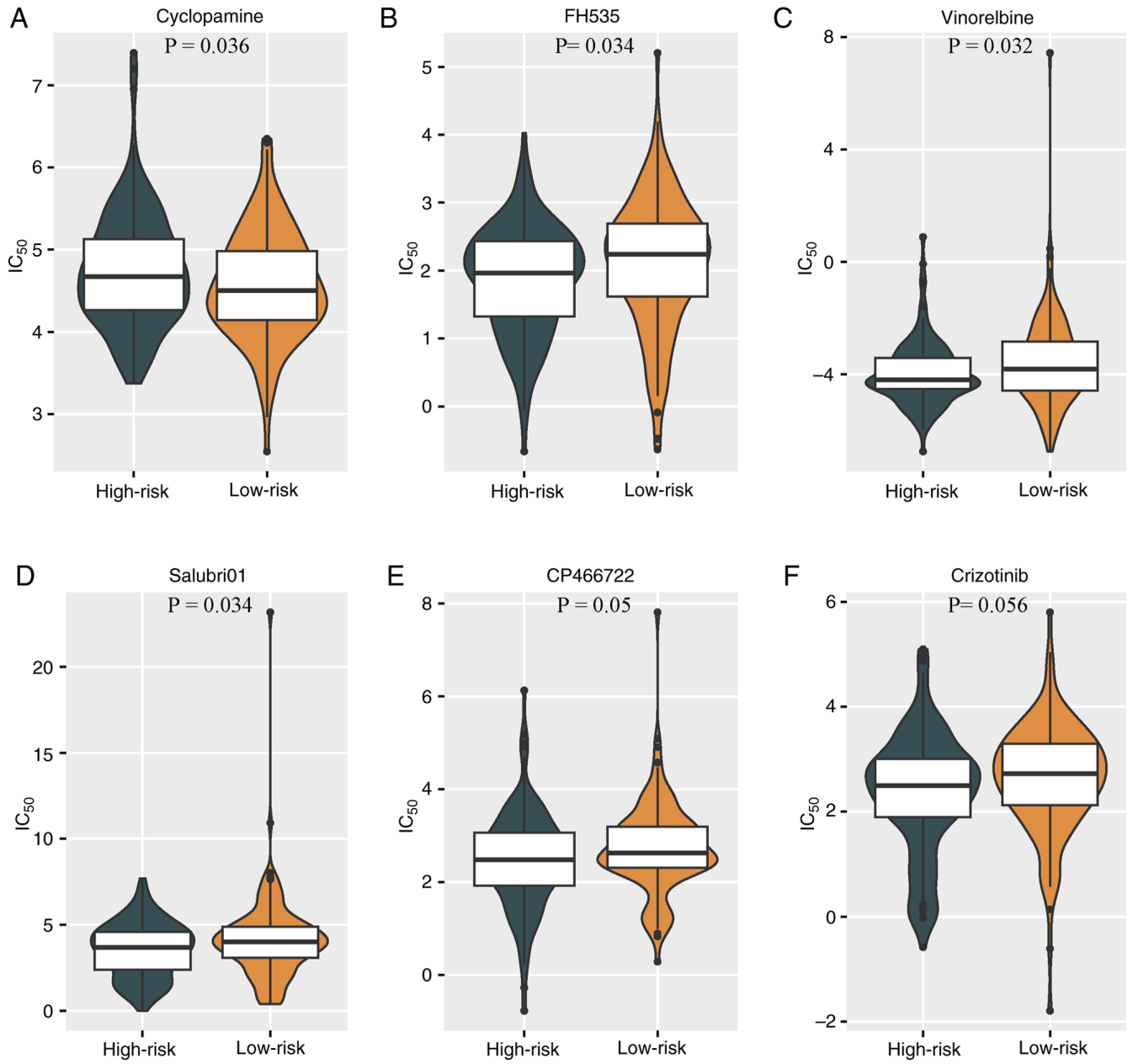


Figure 7. Comparative analysis of drug sensitivity outcomes. (A) Comparative analysis of cyclopamine sensitivity outcomes. (B) Comparative analysis of FH535 sensitivity outcomes. (C) Comparative analysis of vinorelbine sensitivity outcomes. (D) Comparative analysis of Salubri01 sensitivity outcomes. (E) Comparative analysis of CP466722 sensitivity outcomes. (F) Comparative analysis of crizotinib sensitivity outcomes. The high-risk group is shown in green, while the low-risk group is shown in orange. The IC50 values are expressed as mean ± SD. T-test was used to analyze the differences between the two groups.

verified using RT-qPCR aligned with the expression trends of lncRNAs in the datasets, thereby affirming the high caliber and efficacy of RNA-seq data from TCGA and GTEx databases. This corroboration further reiterated the stability of the prognostic model (Fig. 8).

## Discussion

CSCC represents a global public health challenge, with a particularly onerous burden in numerous low- and middle-income countries (28). An IARC study conducted by Singh *et al* (28) compiled incidence and mortality rates of cervical cancer for a decade. Their findings indicated that by 2020, there were an estimated 604,127 cases of cervical cancer worldwide, with 341,831 fatalities (28). Squamous cell carcinoma remains the most prevalent histological type of cervical cancer, accounting for 75-80% of cases, followed by adenocarcinoma, which accounts for 20-25% of cases (29).

Epigenetics refers to alterations in gene expression without modifying the genetic sequence itself (30). Epigenetic modification mechanisms are intimately linked to the development of cervical cancer, with lncRNAs offering advantages for diagnostic and therapeutic applications, rendering them promising targets. A previous study reported a close association between lncRNA dysregulation and the pathological processes underlying cervical intraepithelial neoplasia (31). Hu *et al* (32)

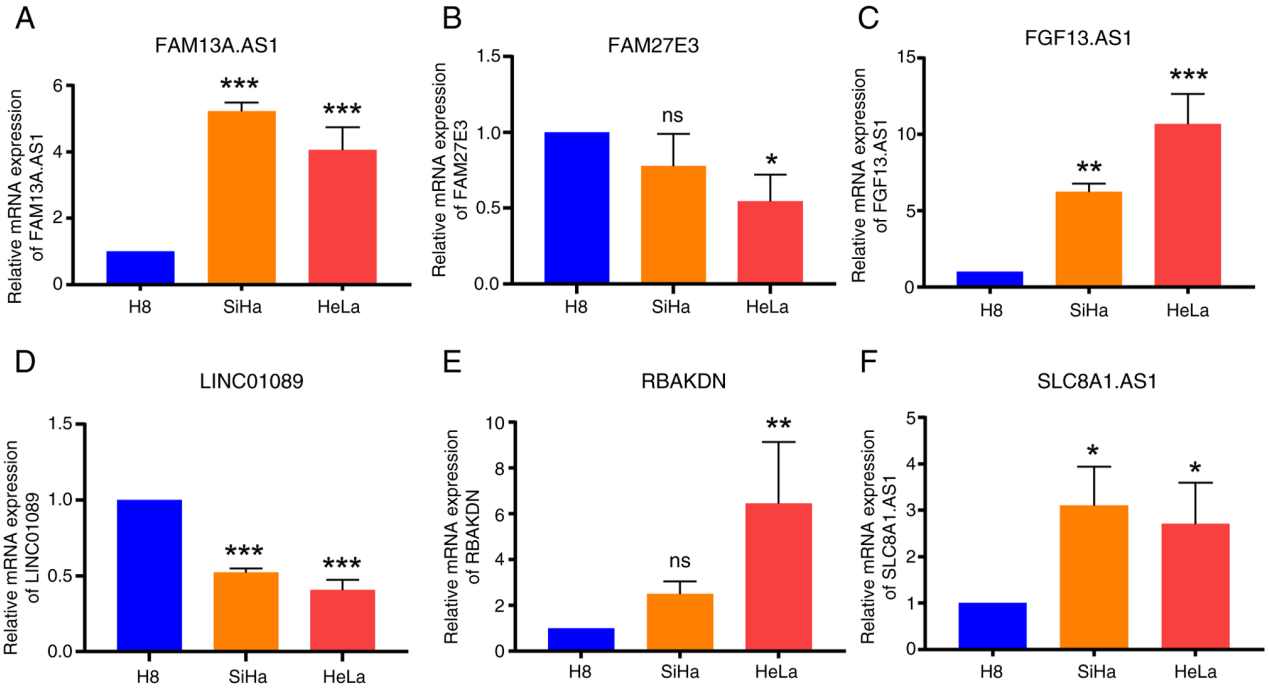


Figure 8. Validation of DELs expression using RT-qPCR. (A-F) Changes in lncRNA expression levels among the cell lines (H8, SiHa and HeLa) were confirmed for FAM13A.AS1, FAM27E3, FGF13.AS1, LINC01089, RBAKDN and SLC8A1-AS1 using RT-qPCR, respectively. $^{*}$P<0.05; $^{**}$P<0.01; $^{***}$P<0.001. The results are expressed as mean ± SD and each experiment was repeated 3 times. lncRNA, long non-coding RNA; DEL, differentially expressed lncRNAs; RT-qPCR, reverse transcription-quantitative PCR.

reported that MIR210HG was upregulated in cervical cancer cells, promoting proliferation and migration through hypoxia-inducible factor 1α. The lncRNA DINO activates the dormant tumor suppressor TP53 via the ATM/checkpoint kinase 2 signaling pathway, thereby inhibiting cervical cancer cell activity (33). In terms of treatment, lncRNAs can influence the sensitivity of cervical cancer to chemoradiotherapy. Zhao *et al* (34) found that LINC00958 could downregulate the radiosensitivity of cervical cancer cells by upregulating ribonucleotide reductase regulatory subunit M2.

RNA methylation modifications represent one of the pivotal post-transcriptional regulatory mechanisms (35). Analysis of public databases by Ji *et al* (36) indicated that various $m^6A$ methylation modification-associated proteins are upregulated, such as programmed cell death ligand 1, in cervical cancer tissues, contributing to carcinogenesis and correlating with elevated programmed death-ligand 1 expression. At present, the $m^7G$ methylation modification regulatory proteins METTL1 and WDR4, which have garnered considerable research attention, are recognized for their role in modulating the course of various tumors (8,12,37-40). However, lncRNAs associated with $m^7G$ have yet to be reported in the pathogenesis of cervical cancer. Consequently, the present study focused on the potential of $m^7G$-related lncRNAs to serve as biomarkers in cervical cancer, which elucidated their role and offered diagnostic and therapeutic insights, as well as the identification of prospective targets for intervention.

Samples included in the present study were sourced from TCGA and GTEx databases, where PCA demonstrated a clear distinction between tumor and normal tissues. Drawing from the GSEA database and extant literature, 35 $m^7G$ methylation regulatory genes were identified. Following differential analysis of these genes and lncRNAs, Pearson's correlation analysis yielded 204 $m^7G$-related lncRNAs. Univariate Cox regression analysis and LASSO regression analysis identified six $m^7G$-related lncRNAs (FAM13A.AS1, FAM27E3, FGF13.AS1, LINC01089, RBAKDN and SLC8A1.AS1). Qiu *et al* (41) observed reduced FAM13A-AS1 expression and elevated levels of miRNA-205-3p in cervical cancer tissues and cell lines (SiHa and HeLa). Upregulation of FAM13A-AS1 expression was found to inhibit the proliferation, migration and invasion of SiHa and HeLa cells, while concurrently increasing apoptosis (41). In renal cancer, lncRNA FAM13A-AS1 can foster the onset of the disease through the FAM13A-AS1/miR-141-3p/NIMA related kinase 6 axis (42). Bioinformatics studies have identified lncRNA FAM13A-AS1 as a prognostic and drug resistance marker in tumors such as neuroblastoma (43) and glioma (44). Although empirical validation is pending, these findings pave the way for future research directions. Previous studies have reported that LINC01089 exerts a key protective effect in a variety of tumors, such as non-small lung cancer (45-48). The predominant mechanisms are largely associated with the competing endogenous RNA network, principally involving pathways such as the LINC01089/miR-27a-3p/tet methylcytosine dioxygenase 1 (45), LINC01089/miR-152-3p/PTEN (46), LINC01089/miR-27b-3p/HOXA10 (47) and LINC01089/miR-27a/secreted frizzled related protein 1 (48) pathways. Among these, the relationship between LINC01089 and miR-27a has been extensively investigated. Li *et al* (49) reported that the LINC01089/miR-27a-3p/BTG axis serves a pivotal role in inhibiting the progression of cervical cancer. Investigations have determined that RBAKDN is principally involved in developmental processes (50). Qin *et al* (51) also identified RBAKDN as an immunologically relevant biomarker

characteristic of predicting early-stage CSCC. SLC8A1.AS1 is closely associated with the biological processes of glioma (52), thyroid carcinoma (53) and oral squamous cell carcinoma (54). FAM27E3 and FGF13.AS1 are still devoid of fundamental research and are primarily utilized in the construction of predictive models. Subsequent validation experiments indicated that, with the exception of a notable decrease in LINC01089 expression, the remaining lncRNAs exhibited a notable increase in cervical cancer cell lines. This finding converges with the outcomes of the aforementioned studies, which indirectly corroborate the results of the present study.

The predictive model constructed based on m$^7$G-related lncRNAs and clinical data was evaluated and Kaplan-Meier analysis demonstrated that the low-risk group had a significantly improved survival prognosis compared with the high-risk group. Although no significant differences were observed between the groups in terms of age, tumor stage or FIGO stage, individual lncRNAs exhibited significant disparities in cervical cancer TNM and FIGO stages, particularly FAM13A.AS1 and LINC01089. This suggested that lncRNAs may be key prognostic indicators, meriting focused attention in future foundational research on cervical cancer. Furthermore, the present study evaluated whether the risk score from the predictive model was an independent prognostic factor for cervical cancer. The HR for the risk prediction model score was 1.10, indicating that the risk prediction model score could serve as an independent prognostic risk factor for cervical cancer. In summary, the model exhibited high sensitivity and specificity in forecasting the prognosis of CSCC, offering valuable theoretical evidence for future clinical applications.

Given the robustness of the present predictive model, it was imperative to assess its clinical translational potential. GSEA demonstrated that the progression of cervical cancer in the high-risk group was closely associated with immune dysregulation. This led to the conjecture that the onset of cervical cancer is closely associated with aberrations in immune responses. Activated mast cells exhibited higher infiltration in the high-risk group, while resting mast cells showed higher infiltration in the low-risk group. Studies have found that activated mast cells in tumor tissues can promote tumor angiogenesis and invasion by releasing classic pro-angiogenic factors (VEGF, fibroblast growth factor 2, platelet-derived growth factor and IL-6), non-classic pro-angiogenic factors (for example, tryptase and chymase) and various matrix metalloproteinases (55,56). The T regulatory cells (Tregs) were higher in the low-risk group. While an increased number of intratumoral Tregs is generally associated with poor prognosis in most cancer types, such as breast cancer, lung cancer, ovarian cancer and hepatocellular carcinoma, elevated Tregs are linked to favorable prognosis in cancer types such as colorectal cancer, estrogen receptor-negative breast cancer, esophageal squamous cell carcinoma and ovarian cancer (57). This discrepancy is primarily due to the phenotypic and functional heterogeneity of Tregs in tumor tissues and studies associating Tregs with favorable prognosis are often conducted in the context of chronic inflammation (57,58). Follicular T cells and CD8$^+$ T cells showed higher infiltration in the low-risk group compared with the high-risk group. Notably, CD8$^+$ T cells are key immune defense cells and their exhaustion is often associated with tumor malignancy (59). In conclusion, findings from the present study may provide insights for future cervical cancer immunotherapy strategies.

Drawing from the results of KEGG analysis, the present study further examined the differences in drug sensitivity between the two groups, which demonstrated that dysregulated transcription, Ras, Rap1 and calcium signaling pathways, among others, were implicated in the progression of high-risk group cervical cancer. The high-risk group exhibited significantly increased responsiveness to the cell cycle inhibitor cyclopamine, whereas the low-risk group exhibited significantly decreased sensitivity to a range of inhibitors, including the Wnt signaling pathway inhibitor FH535, the cell cycle inhibitor vinorelbine, the PP1 inhibitor Salubri01, the serine/threonine-protein kinase inhibitor CP-466722 and the tyrosine kinase receptor inhibitor crizotinib. Cyclopamine and vinorelbine are quintessential cell cycle inhibitory drugs, while crizotinib, a tyrosine kinase receptor inhibitor, has been noted for its relevance due to the upregulation of tyrosine kinase receptors in cervical cancer (60). Crizotinib serves as a potential targeted therapy for cervical cancer (61). CP-466722 hinders ATM kinase activity induced by ionizing radiation and this inhibition is rapidly and fully reversible (62). FH535 acts as a small molecule inhibitor of Wnt/β-catenin signaling and concurrently antagonizes both PPARγ and δ, impeding the aggregation of glutamate receptor interacting protein 1 with β-catenin (63). Salubri01, a PP1 inhibitor, fortifies cells against endoplasmic reticulum stress across various model systems, synergizing markedly with proteasome inhibitors and, to some extent, amplifying apoptosis (64). Notably, vinorelbine has reached a mature stage of clinical application for cervical cancer and is one of the key drugs in chemotherapy regimens for this disease (65). Foundational research on the tyrosine kinase receptor inhibitor crizotinib has demonstrated anticancer activity in cervical cancer cells through the induction of apoptosis (66). Furthermore, the serine/threonine protein kinase inhibitor CP-466722 is known to augment cancer cell sensitivity to radiotherapy, a modality on which cervical cancer treatment is reliant (67). The remaining drugs have not yet been investigated in the context of cervical cancer, underscoring the potential of this predictive model to serve as a key guide in future clinical applications. Overall, the risk model constructed in the present study had notable clinical value. If patients with CSCC can be risk stratified using m$^7$G-related lncRNAs before treatment, it could potentially guide clinicians in making informed choices of therapeutic drugs in the future.

While the stability of the current risk model was corroborated from multiple perspectives, the present study may still harbor limitations. Since the transcriptome expression data and clinical information of the present study subjects were downloaded from the TCGA and GTEx databases, the difference in the number of normal and tumor tissues is a potential limitation of the present study, which may have introduced bias in the statistical analysis of the results. Therefore, further validation through expanded sample sizes in subsequent basic and clinical studies is needed. Additionally, the lncRNAs have only been detected *in vitro*, lacking confirmation through *in vivo* studies and mechanistic experiments. The present study identified m7G-related lncRNAs and developed prognostic, immune infiltration and drug-sensitivity models, contributing to CSCC genotyping, diagnosis and prognosis.

In future studies, the complex and potential molecular regulatory mechanisms involved should be explored. Additionally, experiments interfering with the identified lncRNAs *in vitro* to observe their effects on tumor biological behavior should be performed in addition to the sequencing of cervical cancer tissues prior to treatment to distinguish between high-risk and low-risk groups for clinical drug trials and validation of drug resistance mechanisms through *in vitro* experiments.

**Acknowledgements**

Not applicable.

**Funding**

The present study was funded by the Youth Training Program of Inner Mongolia Medical University (grant no. YKD2021QN042), Science and Technology Million Project Joint Project of Inner Mongolia Medical University [grant no. YKD2020KJBW(LH)006], Construction of Multi-disciplinary Comprehensive System of Clinical Medicine and Tumor in 2023 (grant no. DC2300000607), General Project of Inner Mongolia Medical University (grant no. YKD2021MS015), Inner Mongolia Autonomous Region the Natural Science Foundation of Inner Mongolia (grant no. 2023LHMS08060) and Inner Mongolia Autonomous Region Science and Technology Planning Project (grant no. 2021GG0204).

**Availability of data and materials**

The data generated in the present study may be requested from the corresponding author.

**Authors' contributions**

JZ, YB and YL designed the study and developed the methodology. JZ and YB acquired, analyzed and interpreted the data. JZ and YB performed the experiments. JZ wrote and revised the original draft. ZY collected the data and revised the original draft. YL and ZY confirmed the authenticity of all the raw data. All authors read and approved the final manuscript.

**Ethics approval and consent to participate**

Not applicable.

**Patient consent for publication**

Not applicable.

**Competing interests**

The authors declare that they have no competing interests.

**References**

1. Sung H, Ferlay J, Siegel RL, Laversanne M, Soerjomataram I, Jemal A and Bray F: Global cancer statistics 2020: GLOBOCAN estimates of incidence and mortality worldwide for 36 cancers in 185 countries. CA Cancer J Clin 71: 209-249, 2021.
2. Shanmugasundaram S and You J: Targeting persistent human papillomavirus infection. Viruses 9: 229, 2017.
3. Liu H, Ma H, Li Y and Zhao H: Advances in epigenetic modifications and CC research. Biochim Biophys Acta Rev Cancer 1878: 188894, 2023.
4. Wang T, Kong S, Tao M and Ju S: The potential role of RNA N6-methyladenosine in cancer progression. Mol Cancer 19: 88, 2020.
5. Zhao F, Dong Z, Li Y, Liu S, Guo P, Zhang D and Li S: Comprehensive analysis of molecular clusters and prognostic signature based on m7G-related LncRNAs in esophageal squamous cell carcinoma. Front Oncol 12: 893186, 2022.
6. Luo Y, Yao Y, Wu P, Zi X, Sun N and He J: The potential role of N7-methylguanosine (m7G) in cancer. J Hematol Oncol 15: 63, 2022.
7. Alexandrov A, Martzen MR and Phizicky EM: Two proteins that form a complex are required for 7-methylguanosine modification of yeast tRNA. RNA 8: 1253-1266, 2002.
8. Ying X, Liu B, Yuan Z, Huang Y, Chen C, Jiang X, Zhang H, Qi D, Yang S, Lin S, *et al*: METTL1-m7 G-EGFR/EFEMP1 axis promotes the bladder cancer development. Clin Transl Med 11: e675, 2021.
9. Okamoto M, Fujiwara M, Hori M, Okada K, Yazama F, Konishi H, Xiao Y, Qi G, Shimamoto F, Ota T, *et al*: tRNA modifying enzymes, NSUN2 and METTL1, determine sensitivity to 5-fluorouracil in HeLa cells. PLoS Genet 10: e1004639, 2014.
10. Huang M, Long J, Yao Z, Zhao Y, Zhao Y, Liao J, Lei K, Xiao H, Dai Z, Peng S, *et al*: METTL1-Mediated m7G tRNA modification promotes lenvatinib resistance in hepatocellular carcinoma. Cancer Res 83: 89-102, 2023.
11. Cheng W, Gao A, Lin H and Zhang W: Novel roles of METTL1/WDR4 in tumor via m7G methylation. Mol Ther Oncolytics 26: 27-34, 2022.
12. Deng Y, Zhou Z, Ji W, Lin S and Wang M: METTL1-mediated m7G methylation maintains pluripotency in human stem cells and limits mesoderm differentiation and vascular development. Stem Cell Res Ther 11: 306, 2020.
13. Wang KC and Chang HY: Molecular mechanisms of long noncoding RNAs. Mol Cell 43: 904-914, 2011.
14. Schmitz SU, Grote P and Herrmann BG: Mechanisms of long noncoding RNA function in development and disease. Cell Mol Life Sci 73: 2491-2509, 2016.
15. Long Y, Wang X, Youmans DT and Cech TR: How do lncRNAs regulate transcription? Sci Adv 3: eaao2110, 2017.
16. Guttman M and Rinn JL: Modular regulatory principles of large non-coding RNAs. Nature 482: 339-346, 2012.
17. He J, Huang B, Zhang K, Liu M and Xu T: Long non-coding RNA in CC: From biology to therapeutic opportunity. Biomed Pharmacother 127: 110209, 2020.
18. Cabili MN, Trapnell C, Goff L, Koziol M, Tazon-Vega B, Regev A and Rinn JL: Integrative annotation of human large intergenic noncoding RNAs reveals global properties and specific subclasses. Genes Dev 25: 1915-1927, 2011.
19. Mercer TR, Dinger ME, Sunkin SM, Mehler MF and Mattick JS: Specific expression of long noncoding RNAs in the mouse brain. Proc Natl Acad Sci USA 105: 716-721, 2008.
20. Ravasi T, Suzuki H, Pang KC, Katayama S, Furuno M, Okunishi R, Fukuda S, Ru K, Frith MC, Gongora MM, *et al*: Experimental validation of the regulated expression of large numbers of non-coding RNAs from the mouse genome. Genome Res 16: 11-19, 2006.
21. Iyer MK, Niknafs YS, Malik R, Singhal U, Sahu A, Hosono Y, Barrette TR, Prensner JR, Evans JR, Zhao S, *et al*: The landscape of long noncoding RNAs in the human transcriptome. Nat Genet 47: 199-208, 2015.
22. Brunner AL, Beck AH, Edris B, Sweeney RT, Zhu SX, Li R, Montgomery K, Varma S, Gilks T, Guo X, *et al*: Transcriptional profiling of long non-coding RNAs and novel transcribed regions across a diverse panel of archived human cancers. Genome Biol 13: R75, 2012.
23. Yan X, Hu Z, Feng Y, Hu X, Yuan J, Zhao SD, Zhang Y, Yang L, Shan W, He Q, *et al*: Comprehensive genomic characterization of long non-coding RNAs across human cancers. Cancer Cell 28: 529-540, 2015.
24. Du Z, Fei T, Verhaak RG, Su Z, Zhang Y, Brown M, Chen Y and Liu XS: Integrative genomic analyses reveal clinically relevant long noncoding RNAs in human cancer. Nat Struct Mol Biol 20: 908-913, 2013.
25. Tomikawa C: 7-Methylguanosine modifications in transfer RNA (tRNA). Int J Mol Sci 19: 4080, 2018.

26. Livak KJ and Schmittgen TD: Analysis of relative gene expression data using real-time quantitative PCR and the 2(-Delta Delta C(T)) method. Methods 25: 402-408, 2001.
27. 27.Ritchie ME, Phipson B, Wu D, Hu Y, Law CW, Shi W and Smyth GK: limma powers differential expression analyses for RNA-sequencing and microarray studies. Nucleic Acids Res 43: e47, 2015.
28. Singh D, Vignat J, Lorenzoni V, Eslahi M, Ginsburg O, Lauby-Secretan B, Arbyn M, Basu P, Bray F and Vaccarella S: Global estimates of incidence and mortality of CC in 2020: A baseline analysis of the WHO Global CC elimination initiative. Lancet Glob Health 11: e197-e206, 2023.
29. Small W Jr, Bacon MA, Bajaj A, Chuang LT, Fisher BJ, Harkenrider MM, Jhingran A, Kitchener HC, Mileshkin LR, Viswanathan AN and Gaffney DK: Cervical cancer: A global health crisis. Cancer 123: 2404-2412, 2017.
30. John RM and Rougeulle C: Developmental epigenetics: Phenotype and the flexible epigenome. Front Cell Dev Biol 6: 130, 2018.
31. Gibb EA, Becker-Santos DD, Enfield KS, Guillaud M, van Niekerk D, Matisic JP, Macaulay CE and Lam WL: Aberrant expression of long noncoding RNAs in cervical intraepithelial neoplasia. Int J Gynecol Cancer 22: 1557-1563, 2012.
32. Hu XL, Huang XT, Zhang JN, Liu J, Wen LJ, Xu X and Zhou JY: Long noncoding RNA MIR210HG is induced by hypoxia-inducible factor 1α and promotes CC progression. Am J Cancer Res 12: 2783-2797, 2022.
33. Sharma S and Munger K: Expression of the long noncoding RNA DINO in human papillomavirus-positive CC cells reactivates the dormant TP53 tumor suppressor through ATM/CHK2 signaling. mBio 11: e01190-e01120, 2020.
34. Zhao H, Zheng GH, Li GC, Xin L, Wang YS, Chen Y and Zheng XM: Long noncoding RNA LINC00958 regulates cell sensitivity to radiotherapy through RRM2 by binding to microRNA-5095 in CC. J Cell Physiol 234: 23349-23359, 2019.
35. Wang J, Chew BL, Lai Y, Dong H, Xu L, Balamkundu S, Cai WM, Cui L, Liu CF, Fu XY, *et al*: Quantifying the RNA cap epitranscriptome reveals novel caps in cellular and viral RNA. Nucleic Acids Res 47: e130, 2019.
36. Ji H, Zhang JA, Liu H, Li K, Wang ZW and Zhu X: Comprehensive characterization of tumor microenvironment and m6A RNA methylation regulators and its effects on PD-L1 and immune infiltrates in cervical cancer. Front Immunol 13: 976107, 2022.
37. Chen J, Li K, Chen J, Wang X, Ling R, Cheng M, Chen Z, Chen F, He Q, Li S, *et al*: Aberrant translation regulated by METTL1/WDR4-mediated tRNA N7-methylguanosine modification drives head and neck squamous cell carcinoma progression. Cancer Commun (Lond) 42: 223-244, 2022.
38. Ma J, Han H, Huang Y, Yang C, Zheng S, Cai T, Bi J, Huang X, Liu R, Huang L, *et al*: METTL1/WDR4-mediated m7G tRNA modifications and m7G codon usage promote mRNA translation and lung cancer progression. Mol Ther 29: 3422-3435, 2021.
39. Chen Z, Zhu W, Zhu S, Sun K, Liao J, Liu H, Dai Z, Han H, Ren X, Yang Q, *et al*: METTL1 promotes hepatocarcinogenesis via m7 G tRNA modification-dependent translation control. Clin Transl Med 11: e661, 2021.
40. Liu Y, Zhang Y, Chi Q, Wang Z and Sun B: RETRACTED: Methyltransferase-like 1 (METTL1) served as a tumor suppressor in colon cancer by activating 7-methyguanosine (m7G) regulated let-7e miRNA/HMGA2 axis. Life Sci 249: 117480, 2020.
41. Qiu Z, He L, Yu F, Lv H and Zhou Y: LncRNA FAM13A-AS1 regulates proliferation and apoptosis of cervical cancer cells by targeting miRNA-205-3p/DDI2 axis. J Oncol 2022: 8411919, 2022.
42. Wang XJ, Li S, Fang J, Yan ZJ and Luo GC: LncRNA FAM13A-AS1 promotes renal carcinoma tumorigenesis through sponging miR-141-3p to upregulate NEK6 expression. Front Mol Biosci 9: 738711, 2022.
43. Sugino RP, Ohira M, Mansai SP and Kamijo T: Comparative epigenomics by machine learning approach for neuroblastoma. BMC Genomics 23: 852, 2022.
44. Roh J, Im M, Kang J, Youn B and Kim W: Long non-coding RNA in glioma: Novel genetic players in temozolomide resistance. Anim Cells Syst (Seoul) 27: 19-28, 2023.
45. Guo X and Li M: LINC01089 is a tumor-suppressive lncRNA in gastric cancer and it regulates miR-27a-3p/TET1 axis. Cancer Cell Int 20: 507, 2020.
46. Zhang H, Zhang H, Li X, Huang S, Guo Q and Geng D: LINC01089 functions as a ceRNA for miR-152-3p to inhibit non-small lung cancer progression through regulating PTEN. Cancer Cell Int 21: 143, 2021.
47. Li M and Guo X: LINC01089 blocks the proliferation and metastasis of colorectal cancer cells via regulating miR-27b-3p/HOXA10 axis. Onco Targets Ther 13: 8251-8260, 2020.
48. Li X, Lv F, Li F, Du M, Liang Y, Ju S, Liu Z, Zhou B, Wang B and Gao Y: LINC01089 inhibits tumorigenesis and epithelial-mesenchymal transition of non-small cell lung cancer via the miR-27a/SFRP1/Wnt/β-catenin axis. Front Oncol 10: 532581, 2020.
49. Li S, Han Y, Liang X and Zhao M: LINC01089 inhibits the progression of CC via inhibiting miR-27a-3p and increasing BTG2. J Gene Med 23: e3280, 2021.
50. Liu W, Zhao Y, Liu X, Zhang X, Ding J, Li Y, Tian Y, Wang H, Liu W and Lu Z: A novel meiosis-related lncRNA, Rbakdn, contributes to spermatogenesis by stabilizing Ptbp2. Front Genet 12: 752495, 2021.
51. Qin R, Cao L, Ye C, Wang J and Sun Z: A novel prognostic prediction model based on seven immune-related RNAs for predicting overall survival of patients in early cervical squamous cell carcinoma. BMC Med Genomics 14: 49, 2021.
52. Tomoo Y: Prognostic factors of ovarian cancer at our department. Igaku Kenkyu 57: 154-164, 1987 (In Japanese).
53. Xin Y, Shang X, Sun X, Xu G, Liu Y and Liu Y: SLC8A1 antisense RNA 1 suppresses papillary thyroid cancer malignant progression via the FUS RNA binding protein (FUS)/NUMB like endocytic adaptor protein (Numbl) axis. Bioengineered 13: 12572-12582, 2022.
54. Li Y, Cao X and Li H: Identification and validation of novel long non-coding RNA biomarkers for early diagnosis of oral squamous cell carcinoma. Front Bioeng Biotechnol 8: 256, 2020.
55. Komi DEA and Redegeld FA: Role of mast cells in shaping the tumor microenvironment. Clin Rev Allergy Immunol 58: 313-325, 2020.
56. Liu X, Li X, Wei H, Liu Y and Li N: Mast cells in colorectal cancer tumour progression, angiogenesis, and lymphangiogenesis. Front Immunol 14: 1209056, 2023.
57. Shan F, Somasundaram A, Bruno TC, Workman CJ and Vignali DAA: Therapeutic targeting of regulatory T cells in cancer. Trends Cancer 8: 944-961, 2022.
58. Tzankov A, Meier C, Hirschmann P, Went P, Pileri SA and Dirnhofer S: Correlation of high numbers of intratumoral FOXP3+ regulatory T cells with improved survival in germinal center-like diffuse large B-cell lymphoma, follicular lymphoma and classical Hodgkin's lymphoma. Haematologica 93: 193-200, 2008.
59. Dolina JS, Van Braeckel-Budimir N, Thomas GD and Salek-Ardakani S: CD8+ T cell exhaustion in cancer. Front Immunol 12: 715234, 2021.
60. Muthusami S, Sabanayagam R, Periyasamy L, Muruganantham B and Park WY: A review on the role of epidermal growth factor signaling in the development, progression and treatment of CC. Int J Biol Macromol 194: 179-187, 2022.
61. Boromand N, Hasanzadeh M, ShahidSales S, Farazestanian M, Gharib M, Fiuji H, Behboodi N, Ghobadi N, Hassanian SM, Ferns GA and Avan A: Clinical and prognostic value of the C-Met/HGF signaling pathway in cervical cancer. J Cell Physiol 233: 4490-4496, 2018.
62. Guo K, Shelat AA, Guy RK and Kastan MB: Development of a cell-based, high-throughput screening assay for ATM kinase inhibitors. J Biomol Screen 19: 538-546, 2014.
63. Hsieh MJ, Weng CC, Lin YC, Wu CC, Chen LT and Cheng KH: Inhibition of β-catenin activity abolishes LKB1 loss-driven pancreatic cystadenoma in mice. Int J Mol Sci 22: 4649, 2021.
64. Lu W, Ni K, Li Z, Xiao L, Li Y, Jiang Y, Zhang J and Shi H: Salubrinal protects against cisplatin-induced cochlear hair cell endoplasmic reticulum stress by regulating eukaryotic translation initiation factor 2α signalling. Front Mol Neurosci 15: 916458, 2022.
65. Frenel JS, Mathiot L, Cropet C, Borcoman E, Hervieu A, Coquan E, De La Motte Rouge T, Saada-Bouzid E, Sabatier R, Lavaud P, *et al*: Durvalumab and tremelimumab in combination with metronomic oral vinorelbine for recurrent advanced cervical cancer: An open-label phase I/II study. J Immunother Cancer 13: e010708, 2025.
66. Varma DA and Tiwari M: Crizotinib-induced anti-cancer activity in human cervical carcinoma cells via ROS-dependent mitochondrial depolarization and induction of apoptotic pathway. J Obstet Gynaecol Res 47: 3923-3930, 2021.
67. Jin MH and Oh DY: ATM in DNA repair in cancer. Pharmacol Ther 203: 107391, 2019.